

# Development of a dual-energy computed tomography quality control program: Characterization of scanner response and definition of relevant parameters for a fast-kVp switching dual-energy computed tomography system

Jessica L. Nute\*

*Department of Imaging Physics, The University of Texas MD Anderson Cancer Center, Houston, TX 77030, USA*

Megan C. Jacobsen

*Department of Imaging Physics, The University of Texas MD Anderson Cancer Center, Houston, TX 77030, USA  
Medical Physics Program, The University of Texas MD Anderson Cancer Center UTHealth Graduate School of Biomedical Sciences, Houston, TX 77030, USA*

Wolfgang Stefan

*Department of Imaging Physics, The University of Texas MD Anderson Cancer Center, Houston, TX 77030, USA*

Wei Wei

*Department of Biostatistics, The University of Texas MD Anderson Cancer Center, Houston, TX 77030, USA*

Dianna D. Cody<sup>a)</sup>

*Department of Imaging Physics, The University of Texas MD Anderson Cancer Center, Houston, TX 77030, USA*

(Received 19 April 2017; revised 26 January 2018; accepted for publication 26 January 2018; published 15 March 2018)

**Purpose:** A prototype QC phantom system and analysis process were developed to characterize the spectral capabilities of a fast kV-switching dual-energy computed tomography (DECT) scanner. This work addresses the current lack of quantitative oversight for this technology, with the goal of identifying relevant scan parameters and test metrics instrumental to the development of a dual-energy quality control (DEQC).

**Methods:** A prototype elliptical phantom (effective diameter: 35 cm) was designed with multiple material inserts for DECT imaging. Inserts included tissue equivalent and material rods (including iodine and calcium at varying concentrations). The phantom was scanned on a fast kV-switching DECT system using 16 dual-energy acquisitions (CTDIvol range: 10.3–62 mGy) with varying pitch, rotation time, and tube current. The circular head phantom (22 cm diameter) was scanned using a similar protocol (12 acquisitions; CTDIvol range: 36.7–132.6 mGy). All acquisitions were reconstructed at 50, 70, 110, and 140 keV and using a water-iodine material basis pair. The images were evaluated for iodine quantification accuracy, stability of monoenergetic reconstruction CT number, noise, and positional constancy. Variance component analysis was used to identify technique parameters that drove deviations in test metrics. Variances were compared to thresholds derived from manufacturer tolerances to determine technique parameters that had a nominally significant effect on test metrics.

**Results:** Iodine quantification error was largely unaffected by any of the technique parameters investigated. Monoenergetic HU stability was found to be affected by mAs, with a threshold under which spectral separation was unsuccessful, diminishing the utility of DECT imaging. Noise was found to be affected by CTDIvol in the DEQC body phantom, and CTDIvol and mA in the DEQC head phantom. Positional constancy was found to be affected by mAs in the DEQC body phantom and mA in the DEQC head phantom.

**Conclusion:** A streamlined scan protocol was developed to further investigate the effects of CTDIvol and rotation time while limiting data collection to the DEQC body phantom. Further data collection will be pursued to determine baseline values and statistically based failure thresholds for the validation of long-term DECT scanner performance. © 2018 American Association of Physicists in Medicine [https://doi.org/10.1002/mp.12812]

Key words: computed tomography, dual-energy CT, quality control, spectral imaging

## 1. INTRODUCTION

Currently, the standard for routine quality control of single-energy computed tomography (SECT) is set by the American

College of Radiology (ACR) in its CT QC Manual.<sup>1</sup> It recommends daily artifact analysis and monitoring of the mean and standard deviation of the CT number of water. While this document represents an excellent standard for use with SECT

imaging, little attention has been paid to quality control of clinical dual-energy CT (DECT) systems. These scanners often incorporate more advanced hardware, such as the fast-kVp switching system used by GE<sup>2</sup> or the split-filter system both used by Siemens, or the dual-layer detector system used by Philips.<sup>3,4</sup> In addition, dual-energy CT scanners produce distinct image types such as virtual monoenergetic, virtual noncontrast and material density images that are unique to DECT imaging.<sup>5,6</sup> Neither the capabilities of this hardware nor the consistency of these unique image types can be monitored using a single-energy quality control program.

Since the release of the first clinical dual-energy CT scanner in 2006,<sup>3</sup> many studies have investigated the growing range of dual-energy hardware and software solutions as well as the novel data produced by them. Of particular interest was the use of the virtual monoenergetic reconstructions, which allow the user to vary the image contrast by selecting the virtual keV of the reconstruction and thus the relative influence of photoelectric and Compton processes.<sup>7–9</sup>

Monoenergetic reconstructions have been evaluated for iodine contrast-to-noise ratio (CNR),<sup>10–12</sup> noise equivalence to SECT,<sup>10,12–15</sup> NPS across keV,<sup>13</sup> spatial resolution,<sup>13</sup> and low-contrast detectability.<sup>16</sup> Due to the theoretical reduction in beam hardening possible with dual-energy techniques,<sup>6–9</sup> higher energy monoenergetic images have been investigated for their reduction in beam hardening from bone,<sup>14,17</sup> as well as reduction in metal artifact.<sup>18–22</sup>

Since dual-energy CT has the potential to be used in a quantitative fashion, it is vital to validate the attenuations derived from monoenergetic reconstructions as well as the material concentrations derived from material density images. Of particular interest has been the quantification of iodine, either using calculated concentration<sup>23–26</sup> or enhancement<sup>6,27,28</sup> based on concentration values from a material density image provided by GE systems or iodine overlay images provided by Siemens systems, respectively.<sup>13,29</sup> In general, measurements of iodine concentration and enhancement were found to be highly correlated with true iodine concentration.<sup>23,25,29,30</sup> Iodine quantification error was shown to vary based on position within a phantom by Zhang et al.,<sup>13</sup> however the opposite was found by Matsuda et al.<sup>29</sup> It is worth noting, however, that Matsuda et al. evaluated iodine quantification solely based on a 65 keV monoenergetic reconstruction and not with material density images. Iodine quantification error was also shown to increase with increasing phantom size;<sup>25</sup> however, this effect has been disputed by other studies.<sup>6,23,29</sup> Evaluation of the CT number stability for monoenergetic reconstructions has shown dependence on phantom size, as well as greater inaccuracies for dense materials in low keV reconstructions.<sup>30,31</sup> This effect may be due to suboptimal correction of beam hardening effects for these energies. The presence of tin filtration has also been shown to affect the CT numbers from monoenergetic reconstructions created using the Siemens systems.<sup>27,28</sup>

While these studies have shed light on the characterization of these dual-energy CT systems, evaluation has yet to be performed on multiple scanners over time in order to lay the

framework for a dual-energy quality control (DEQC) process. A number of steps must be taken in order to work toward a pertinent and clinically implementable DEQC process. First, the system response must be characterized through exploratory research using a comprehensive phantom and a wide range of acquisition parameters, phantom inputs and test metrics, isolating a subset worthy of continued study. Second, long-term data collection should be pursued to determine relative failure rates and establish limits based on clinical endpoints. Finally, a streamlined phantom and protocol can be designed that targets the acquisition parameters, phantom inputs, and test metrics shown to be tied to scanner performance, while allowing for ease of implementation in a typical clinical setting. To that end, this paper targets the first of the three steps through the development of a prototype exploratory phantom system and protocol for extensive data collection using a fast kV-switching DECT system.

## 2. MATERIALS AND METHODS

### 2.A. Prototype phantom design

In order to investigate both body-specific and neuro-specific challenges and acquisition techniques as part of our investigation, a two-part prototype phantom was designed (Fig. 1). The outer shape of the phantom was elliptical to approximate the shape of the human torso. The phantom was designed to mimic the body habitus of a larger patient with an equivalent diameter of approximately 35 cm. This elliptical body phantom contained an insert which could be removed for separate scanning with neuro specific Gemstone Spectral Imaging (GSI) presets, which define fixed combinations of technique parameters available in dual-energy mode. When separate from the body phantom, this insert is referred to as the “DEQC head phantom”. Both the DEQC body and head phantoms were constructed from a uniform epoxy resin-based background material (of approximately 22 HU at 120 kVp) with a high-density polyethylene (HDPE) slip-ring between the head insert and the larger body phantom.

#### 2.A.1. Material inserts

Given the exploratory nature of the investigation, a variety of tissue and material inserts were included in the DEQC phantom (Table I). These inserts, unlike the materials traditionally used in SECT phantoms, were designed to be spectrally equivalent across the range of virtual keVs simulated in DECT. Insert compositions and concentrations were chosen based on their applicability to current clinical and research applications of DECT. While this variety of inserts allowed for the evaluation of a range of clinically relevant endpoints, including virtual calcium removal, iron and iodine differentiation, material density linearity and effective Z estimation, a smaller subset of inserts were used to evaluate possible DEQC test metrics.

The arrangement of the inserts within the phantom is shown in Fig. 1 and was determined based on the reduction

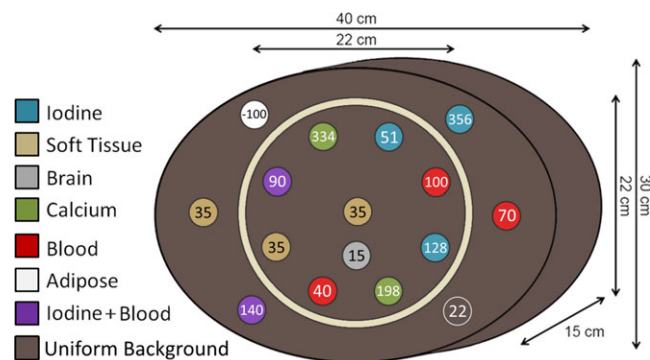


FIG. 1. Basic structure and dimensions of DEQC phantom with DEQC insert layout showing average 120 kVp HU level of inserts.

of beam hardening and test metric considerations (see below). The insert rods measure 2.8 cm in diameter and extend the entire 15 cm length of the phantom to ensure that data incorporated in the image due to helical overranging did not include any air gaps or background material. Both material and tissue equivalent inserts detailed in Table I were developed and manufactured in conjunction with Gammex, Inc (Middleton, WI, USA).

All inserts underwent both quantitative and qualitative testing to ensure uniformity, accuracy, and, if needed, inter-comparability. Any inserts not uniform to within 2 HU along the z-axis or showing any visible defects were returned to the vendor for replacement. The three soft tissue inserts included in the phantom were further validated to verify that they were interchangeable based on both their single-energy attenuation data and dual-energy spectral curves.

**2.B. Test metrics**

Decades of SECT use has led to the identification of a core group of evaluations necessary for routine verification of SECT scanner performance. The 2012 ACR CT quality

control manual<sup>1</sup> outlines the necessary evaluations for daily single-energy CT quality control: standard deviation of water (image noise), mean CT# of water (absolute CT number accuracy), and artifact analysis (detector uniformity). While both hardware and software differences set dual-energy CT scanners apart from traditional single-energy CT scanners, these tests provide the basis for our development of a dual-energy CT quality control program.

While certain test metrics would undoubtedly benefit from a more uniform phantom, the exploratory DEQC phantom system was designed to allow for a wide range of dual-energy investigation, limiting the ability to generate a large uniform area. Given the constraints of a heterogeneous phantom model, as well as the unique capabilities and imaging concerns involved in DECT imaging, modifications were made to these standard single-energy QC tests.

Noise in CT images is usually assessed over a large ROI in a uniform phantom; however, due to the constraints of our phantom model, noise was assessed as the standard deviation within the brain insert in the head phantom portion of the DEQC phantom system. This insert is present during both body phantom and separate head phantom scanning and is the insert with the SECT attenuation (HU) closest to water (15 HU vs. 0 HU). This noise test metric was applied to both monoenergetic and material density image types.

Due to the ability of DECT to create virtual monoenergetic data visualizations at a variety of different keV levels, the concept of absolute CT number accuracy is more complicated. While it is expected that monoenergetic reconstructions at different keVs will result in different CT numbers, it is assumed that variations in technique parameters would not affect these values. In order to assess the effect of technique parameters on the monoenergetic CT numbers, a new test metric, monoenergetic HU stability, was developed. This metric describes the stability of the monoenergetic CT numbers with respect to technique parameter variation and was defined as the average CT number over all voxels within the

TABLE I. List of DEQC phantom insert types.

Insert	Compound	HU at 120 kVp	Electron density	Effective Z <sup>a</sup>	Biology modeled
Blood	Fe <sub>2</sub> O <sub>3</sub>	40	1.033	6.392	Blood
Blood	Fe <sub>2</sub> O <sub>3</sub>	70	1.068	6.350	Clot (Normal)
Blood	Fe <sub>2</sub> O <sub>3</sub>	100	1.102	6.309	Clot (Extreme)
Calcium	CaCO <sub>3</sub>	198	1.128	6.757	Calcification
Calcium	CaCO <sub>3</sub>	334	1.191	7.380	Bone
Iodine 2 mg/mL	C <sub>6</sub> H <sub>5</sub> I	51	1.002	6.306	NA
Iodine 5 mg/mL	C <sub>6</sub> H <sub>5</sub> I	128	1.003	6.441	NA
Iodine 15 mg/mL	C <sub>6</sub> H <sub>5</sub> I	356	1.008	6.891	NA
Iodine enhancement	Fe <sub>2</sub> O <sub>3</sub> + C <sub>6</sub> H <sub>5</sub> I	40 + 50	1.034	6.478	Typical enhancement threshold for neuro studies
Iodine enhancement	Fe <sub>2</sub> O <sub>3</sub> + C <sub>6</sub> H <sub>5</sub> I	40 + 100	1.035	6.568	Typical enhancement threshold for thoracic studies
Soft tissue	NA	35	1.029	6.305	Soft tissue
Adipose	NA	-100	0.944	5.985	Adipose
Brain	NA	15	1.022	6.423	Brain

<sup>a</sup>Effective Z calculation based on elemental composition of each material as provided by Gammex.

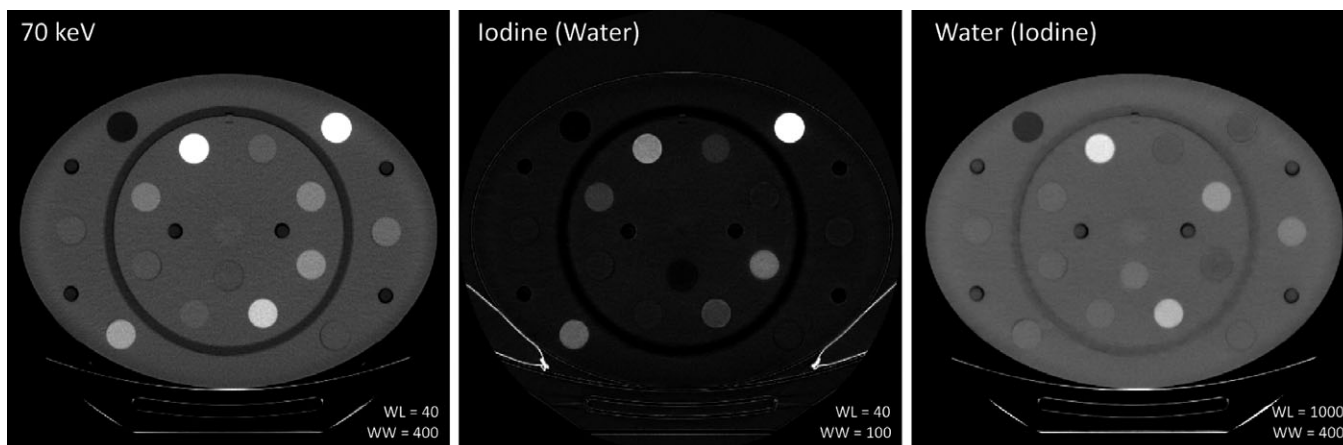


FIG. 2. DECT images of the DEQC body phantom for 70 keV monoenergetic reconstruction and Iodine (Water) and Water (Iodine) material density images. Note the high signal from both the iodine and calcium rods due to the presence of high-Z elements.

three soft tissue rods in the DEQC phantom. This definition provided positional independence due to the spacing of the soft tissue rods within the phantom (Fig. 2) as well as basing the metric in a clinical CT number range (approximately 35 HU). To allow for the verification of Monoenergetic HU Stability at various points along the dual-energy spectral curve, four keV energy levels were chosen to evaluate this metric: 50, 70, 110, and 140 keV.

In addition to the tests described above, an evaluation of uniformity was also included. While uniformity is typically defined in a uniform phantom, the heterogeneity of our DEQC phantom required modification of this classical definition. Soft tissue rods were positioned at the center of the DEQC phantom, periphery of the DEQC head phantom and periphery of the DEQC body phantom (Fig. 1). To minimize the potential of beam hardening from linearly positioned inserts, the head phantom peripheral inserts were offset from the body phantom peripheral inserts. Positional constancy was then defined as the mean ROI value of the most peripheral soft tissue rod minus the mean ROI value of the central soft tissue rod. It was assessed on both monoenergetic and material density image types. Both water and iodine material density images were assessed due to the differing influence of the 80 and 140 kV acquisitions on these image types. Water density images have a higher percent contribution from the higher 140 kV beam, while iodine density images have a higher percent contribution from the lower 80 kV beam. Given that the two beam spectra would likely be affected by phantom (or patient) size and beam hardening to different extents, the collection of positional constancy data using both water and iodine density images was pursued.

While SECT QC can help inform DECT QC, the introduction of material density-based imaging necessitates additional quality control metrics unique to these image types. In DECT, the process of material decomposition is used to create paired material density images which display the

densities of two different materials that together would mimic the attenuation properties of the target material or tissue.<sup>2,5</sup> These material density images are expressed in units of mg/mL and, unlike Hounsfield numbers, are absolute measures of a physical quantity associated with the material or tissue. These values can be quantitative if the material is made solely of the two compounds present in the material basis pair. For example, a water/iodine material decomposition of a solution of iodine and water should yield accurate results for both the water density in the water material image and iodine density in the iodine material image. It is important to note, however, that an insert containing materials other than iodine and water would still be decomposed into the two basis materials. For example, an insert containing polyethylene and calcium would contribute signal to both the water and iodine images, and thus may have measurable values present in both iodine and water images even though no water or iodine was present in the insert. In this case, the material density images cannot be evaluated quantitatively and serve only as a qualitative mapping of the low-Z to high-Z contributions to the overall attenuation of the material.

In order to test the quantitative accuracy of the water/iodine material decomposition, three inserts consisting solely of spectrally equivalent solid water and iodine were included in the DEQC phantom, each with a different known density of iodine:  $2.0 \pm 0.1$  mg/mL,  $5.0 \pm 0.2$  mg/mL, and  $15 \pm 0.5$  mg/mL (written communication, Gammex). The quantification of the measured concentration on an iodine material density image — from an iodine/water basis pair — was then compared to the known iodine concentration for each rod and the error calculated. This value was investigated as both absolute error and percent error relative to the known iodine material concentration for each of the three rods.

Test metrics included in the DEQC program are detailed in Table II, including their application to relevant image types.



TABLE II. DEQC program test metrics.





Test metric	Noise	Monoenergetic HU stability	Iodine quantification error	Positional constancy
Rod composition	Brain	Soft tissue	Iodine	Soft tissue
Rod position				
Image type				
50 keV	X	X		X
70 keV	X	X		X
110 keV	X	X		X
140 keV	X	X		X
Iodine (Water)	X		X	X
Water (Iodine)	X			X

TABLE III. Head phantom DEQC protocol version 1.

Acquisitions	GSI-preset	Pitch	Rotation time (s)	mA	CTDI <sub>vol</sub> (mGy)	Image thickness (mm)
1, 2	GSI-26	0.531	0.7	375	67	1.25, 3.75
3, 4	GSI-26	0.969	0.7	375	36.7	1.25, 3.75
5, 6	GSI-20	0.531	0.5	630	81.4	1.25, 3.75
7, 8	GSI-20	0.969	0.5	630	44.6	1.25, 3.75
9, 10	GSI-9	0.531	0.9	600	132.6	1.25, 3.75
11, 12	GSI-9	0.969	0.9	600	72.7	1.25, 3.75

Note: All acquisitions used helical scan mode, beam width of 20 mm, Head SFOV, DFOV of 25 cm, and Standard reconstruction algorithm. A total of five images were acquired per acquisition.

### 2.C. DEQC protocol version 1: Identification of relevant technique parameters

Unlike single-energy acquisitions, where the various technique parameters can be modified individually, dual-energy acquisitions using the GE 750HD CT system (GE Healthcare, Waukesha, WI, USA) are limited to a number of GSI-presets wherein the bowtie filter, collimation, rotation time, and mA (and thus CTDI<sub>vol</sub>) are fixed. Protocols were therefore designed using a range of GSI-presets to allow for variation in CTDI<sub>vol</sub>, rotation time, pitch, and image thickness across both the DEQC head (Table III) and body protocols (Table IV). Image thickness values were selected for their clinical applicability. CTDI<sub>vol</sub> values were selected to span the wide range of dose levels achievable using the pitch values under investigation and the GSI-presets available on the scanner (minimum: 9 mGy, maximum: 62 mGy), and should not be taken to imply that these values are clinically acceptable. The range included higher doses to enhance the consistency of the image quality and reduce variability in the data in order to more easily identify small deviations in the results. These protocols were used to scan both the DEQC head and body phantoms a total of 28 times over the course of 2 weeks on 10 different GE 750HD CT scanners.

Based on the DEQC program test metrics, a number of dual-energy reconstructions were performed, including both

TABLE IV. Body phantom DEQC protocol version 1.

Acquisition	GSI-preset	Pitch	Rotation time (s)	mA	CTDI <sub>vol</sub> (mGy)	Image thickness (mm)
1, 2	GSI-36	0.516	0.8	260	19.6	2.5, 5
3, 4	GSI-36	0.984	0.8	260	10.3	2.5, 5
5, 6	GSI-1	0.516	0.5	630	33.9	2.5, 5
7, 8	GSI-1	0.984	0.5	630	17.8	2.5, 5
9, 10	GSI-10	0.516	0.8	600	48.6	2.5, 5
11, 12	GSI-10	0.984	0.8	600	25.5	2.5, 5
13, 14	GSI-5	0.516	1	600	62	2.5, 5
15, 16	GSI-5	0.984	1	600	32.5	2.5, 5

Note: All acquisitions used helical scan mode, beam width of 40 mm, Large Body SFOV, 42 cm DFOV, and Standard reconstruction algorithm. A total of five images were acquired per acquisition.

monoenergetic and material density image types (Table II, Fig. 2). For all reconstructions, the minimum number of images allowable was created to facilitate data transmission and storage. The minimum number of images allowed using a material density reconstruction was one, while monoenergetic reconstructions required the full image set (5 images) to be reconstructed.

#### 2.C.1. Statistical analysis and visualization

For the central image in each DEQC phantom acquisition, mean and standard deviation data were collected for each rod using Matlab (Version 2014a, MathWorks). Test metrics were calculated for appropriate image types for both the DEQC head and body phantom. The ROI summary statistics, as well as the results of the test metrics were then written out to a text file for all images and exams.

A linear mixed model was used to compare primary endpoints (Positional Constancy, Noise, Monoenergetic HU Stability, and Iodine Quantification Error) between technique parameters (CTDI<sub>vol</sub>, Pitch, Rotation Time, Image Thickness). The mixed model took into account the correlation between measurements from the same scanner. Pairwise comparisons between imaging settings were carried out if the

overall likelihood ratio test was significant. Tukey–Kramer adjustment was used to control family-wise type I error rate at 5% for all pairwise comparisons in each model. All tests were two-sided and p-values of 0.05 or less were considered statistically significant. Statistical analysis was carried out using SAS version 9 (SAS Institute, Cary, NC, USA). Factors with statistically significant impact on primary endpoints were identified and selected for further analysis.

While statistical significance can be a useful tool, it is wise to consider the tolerances established for the system. In other words, a 1 HU difference may be statistically significant; however, if the manufacturer tolerance allows an error of more than 3 HU, then the difference would not be considered nominally significant. Therefore, statistically significant changes in test metrics were then compared against the manufacturer’s specifications for the system. Test metrics that resulted in changes above the expected variance in the system were then identified as nominally significant.

Given the lack of dual-energy tolerances, either stated by manufacturers or in the literature, tolerances were based on those for single-energy acquisition. The technical reference manual for the GE 750 HD<sup>32</sup> states that the CT number of water is in tolerance if it is within 3 HU of its reference value. Since monoenergetic images are expected to present the same quantitative precision as traditional single-energy CT images, this tolerance was extended to the 50, 70, 110, and 140 keV images.

This threshold was extended to water (iodine) images based on the understanding that an increase in 3 HU correlates with an increase from 1,000 mg/mL of water to 1,003 mg/mL of water. Although iodine (water) images are technically derived from the same base data as the water (iodine) and monoenergetic images, these images are used not only quantitatively but also directly represent the physical concentration of a material, and thus must not only be precise but also accurate. No tolerance for either the precision or the accuracy of iodine (water) images could be found in GE documentation. Written communication with the manufacturer provided an internal tolerance of  $\pm 1$  mg/mL for a 5 mg/mL iodine solution scanned at 36.34 mGy. Considering the wide range of iodine concentrations investigated and the unknown effect of dose on iodine accuracy, the tolerance was expanded to consider both a fixed error of  $\pm 1$  mg/mL and a percentage error of 10%. A summary of the nominal significance criteria can be seen in Table V.

Factors identified as both statistically and nominally significant were then used to inform the development of the DEQC protocol version 2 for scanner characterization.

TABLE V. Nominal significance criteria based on image type and evaluation in question.

Image type/evaluation	Error threshold
Monoenergetic	>3 HU
Water (Iodine)	>3 mg/mL
Iodine (Water)	>1 mg/mL
Iodine quantification error	>10% or >1 mg/mL (whichever greater)

## 2.D. DEQC protocol version 2: Scanner characterization

After the initial data collection based on DEQC protocol version 1, a second protocol version was developed to target those factors found influential while removing those not warranting further investigation. To further separate the effects of rotation time and dose, GSI-presets with similar CTDI<sub>vol</sub> values but differing rotation times were included. Three such groups were found among the body GSI-presets, while only one dose matched pair was found among the head GSI-presets. Pitch was varied solely to provide additional variation in CTDI<sub>vol</sub> across the limited GSI-preset options. Image thickness was reduced to a single value across both DEQC head and body phantom protocols to allow for more direct comparison of DEQC results across the two phantoms. A 5 mm thickness was selected due to its clinical applicability and reduced noise. The updated DEQC head and body phantom protocols are shown in Tables VI and VII. Dual-energy reconstructions were performed identically as in protocol version 1.

Weekly DEQC scans were performed on ten GE 750HD CT scanners over a 13-week period in order to characterize the test metric dependence on technique parameters in order to inform the creation of a streamlined DEQC protocol appropriate for clinical implementation.

### 2.D.1. Statistical analysis and visualization

Automated ROI placement was carried out in a similar manner as that described in 2.C.1, resulting in the mean and standard deviation data from each rod. A MySQL database (Oracle, Redwood City, CA, USA) and Python script were employed to allow further automation for the more extensive data collection. Summary statistics of primary endpoints (Positional Constancy, Noise, Monoenergetic HU Stability, and Iodine Quantification Error) were analyzed using variance component analysis. Noise was transformed to the logarithmic scale before statistical modeling due to right skewness. Variance component analysis was also used to estimate random error in the data.

Variance was estimated based on technique parameters including mA, rotation time, mAs and CTDI<sub>vol</sub>. These variance contributions were then compared to that from random error, and those technique parameters with variance contributions greater than random error were identified as major variance contributors. Rotation time and mA were analyzed separately from mAs to ensure that neither factor was solely responsible for variance contributions attributed to mAs. Statistical analysis was carried out using SAS version 9 (SAS Institute, Cary, NC, USA).

The variance from those parameters identified as major variance contributors were then transformed to a 95% confidence interval defined as twice the square root of the variance. This transformation enabled manufacturer tolerances to be applied and nominal significance of the effect to be assessed. For example, if there was a 95% chance a new data point would fall between  $-1$  and  $1$  HU, and the manufacturer

TABLE VI. DEQC head phantom protocol version 2.

Acquisition	GSI-preset	Pitch	Rotation time (s)	mA	mAs	CTDI <sub>vol</sub> (mGy)	Image thickness (mm)
1	GSI-30	0.531	0.8	550	440	105.6	5
2	GSI-20	0.531	0.5	630	315	81.4	5
3	GSI-26	0.531	0.7	375	262.5	67	5
4	GSI-19	0.969	0.6	640	384	54.7	5
5	GSI-39	0.531	0.8	208	166.4	47.8	5
6	GSI-20	0.969	0.5	630	315	44.6	5
7	GSI-26	0.969	0.7	375	262.5	36.7	5
8	GSI-39	0.969	0.8	208	166.4	26.2	5

Note: All acquisitions used helical scan mode, 20 mm beam width, Head SFOV, 25 cm DFOV, and Standard reconstruction algorithm.

TABLE VII. DEQC body phantom protocol version 2.

Acquisition	GSI-preset	Pitch	Rotation time (s)	mA	mAs	CTDI <sub>vol</sub> (mGy)	Image thickness (mm)
1	GSI-5	0.516	1	600	600	62	5
2	GSI-10	0.516	0.8	600	480	48.6	5
3	GSI-1	0.516	0.5	630	315	33.9	5
4	GSI-5	0.984	1	600	600	32.5	5
5	GSI-10	0.984	0.8	600	480	25.5	5
6	GSI-1	0.984	0.5	630	315	17.8	5
7	GSI-54	0.516	0.6	275	165	17.4	5
8	GSI-48	0.516	0.7	260	182	17.2	5
9	GSI-51	0.984	0.5	360	180	10.3	5
10	GSI-36	0.984	0.8	260	208	10.3	5

Note: All acquisitions used helical scan mode, 40 mm beam width, Large Body SFOV, 42 cm DFOV, and Standard reconstruction algorithm.

tolerance is from  $-3$  to  $3$  HU, then that technique parameter, although potentially a major variance contributor, is not considered nominally significant.

While statistical analysis is useful in identifying factors that have a substantial impact, and manufacturer tolerances are useful in determining if that impact is nominally significant, neither sheds light on the manner of impact the factor has on the endpoint in question. To this end, technique parameters identified as both major variance contributors and having a nominally significant effect on the test metric were then graphed.

### 3. RESULTS

#### 3.A. DEQC protocol version 1: Identification of relevant technique parameters

Results of the linear mixed model for the version 1 data from the DEQC body phantom are shown in Table VIII. Values represent the maximum impact from modifying the technique parameter in question within the range investigated by the DEQC protocol (Table IV). For example, the monoenergetic HU stability for 50 keV images may vary by as much as 14.45 HU depending on the choice of CTDI<sub>vol</sub> within the

range of 10.3–62 mGy. Values in bold represent cases where the technique parameter was found to have a statistically significant effect on the test metric and image type in question. Underlined values represent outcomes that exceed our nominal significance criteria (Table V).

While statistically significant, changes in technique parameters did not have a nominally significant effect on iodine quantification error for any of the iodine concentrations investigated. Both CTDI<sub>vol</sub> and rotation time were found to have statistically and nominally significant effects on monoenergetic HU stability, image noise, and positional constancy. Pitch and image thickness were found to only affect image noise at both the statistically and nominally significant levels. Effects of technique parameters on monoenergetic HU stability and positional constancy were reduced for 70 keV reconstructions.

Based on these results, CTDI<sub>vol</sub> and rotation time were identified as scan parameters worthy of further investigation. The effect of image thickness on image noise is well understood<sup>33</sup> and the effects of pitch can be easily explained by the large differences in CTDI<sub>vol</sub> between the two pitch settings evaluated. Results for the DEQC head phantom (data not shown) were remarkably similar, however showed a reduced impact of all technique parameters across all test metrics.

TABLE VIII. Maximum impact of technique parameter on test metrics for the DEQC body phantom (Protocol 1).

Test metric	Image type	Units	CTDIvol	Rotation time	Pitch	Image thickness	
Iodine quant error 2 mg/mL	I(Wa)	mg/mL, %	<b>0.22, 10.77%</b>	<b>0.11, 5.59%</b>	<b>0.03, 1.33%</b>	0.02, 1.23%	
Iodine quant error 5 mg/mL	I(Wa)	mg/mL, %	<b>0.32, 6.35%</b>	<b>0.18, 3.70%</b>	<b>0.04, 0.85%</b>	0.00, 0.01%	
Iodine quant error 15 mg/mL	I(Wa)	mg/mL, %	0.16, 1.06%	<b>0.10, 0.65%</b>	0.02, 0.12%	0.16, 0.05%	
Monoenergetic HU stability	50 keV	HU	<u>14.45</u>	<u>8.26</u>	0.16	0.11	
	70 keV	HU	<u>2.1</u>	<u>1.3</u>	<b>0.22</b>	0.07	
	110 keV	HU	<u>5.79</u>	<u>2.86</u>	0.4	0.04	
	140 keV	HU	<u>7.43</u>	<u>3.78</u>	0.44	0.04	
	50 keV	HU	<b>34.35</b>	<b>10.78</b>	<b>11.48</b>	<b>10.36</b>	
Noise	70 keV	HU	<u>16.51</u>	<u>5.06</u>	<u>6.22</u>	<u>5.62</u>	
	110 keV	HU	<u>14.47</u>	<u>4.56</u>	<u>4.77</u>	<u>4.22</u>	
	140 keV	HU	<u>13.55</u>	<u>4.35</u>	<u>4.32</u>	<u>3.76</u>	
	I(Wa)	mg/mL	<u>5.43</u>	<u>1.77</u>	<u>1.61</u>	<u>1.39</u>	
	Wa(I)	mg/mL	<u>12.81</u>	<u>4.22</u>	<u>3.81</u>	<u>3.21</u>	
	Positional constancy	50 keV	HU	<u>10.26</u>	<u>9.24</u>	0.57	0.52
		70 keV	HU	<b>0.89</b>	0.22	0.25	0.12
110 keV		HU	<u>5.76</u>	<u>5.67</u>	0.03	0.44	
140 keV		HU	<u>7.04</u>	<u>6.91</u>	0.08	0.52	
I(Wa)		mg/mL	<u>0.36</u>	<u>0.34</u>	0.01	0.02	
Wa(I)	mg/mL	<u>8.85</u>	<u>8.68</u>	0.14	0.67		

Note: Values in bold were identified as statistically significant while those underlined were identified as both statistically and nominally significant.

### 3.B. DEQC protocol version 2: Scanner characterization

The results of the variance component analysis from protocol 2 are shown in Table IX. Technique parameters found to have a major contribution to the overall variance (variance greater than the calculated random error) for a combination of test metric and image type are listed. While variance component analysis on the natural log of noise allowed for the comparison of the variances from random error and various technique parameters, it did not allow for the direct calculation of a 95% CI. Therefore, the effect of technique parameters on noise could not be assessed for nominal significance due to the transformation applied to the data. Nominal significance is thus limited to interpretation of the graphical visualizations of the raw data.

Based on this analysis, mAs was identified as a major variance contributor to monoenergetic HU stability for both the DEQC head and body phantoms. For the DEQC body phantom, the effect of mAs on monoenergetic HU stability was found to be nominally significant for all image types except 70 keV, while for the DEQC head phantom, the effect was only nominally significant for 110 and 140 keV.

For the DEQC body phantom, mAs was identified as a major variance contributor to positional constancy for all image types except for 70 keV, and the effect was nominally significant in all image types except 70 keV and iodine (water). In contrast, mA was identified as a major variance contributor to positional constancy for the DEQC head phantom; however, the effect was not nominally significant for any image type.

CTDIvol was identified as a major variance contributor to noise for both phantoms and all image types. In addition to CTDIvol, mA was also identified as a major variance

contributor to noise for the DEQC head phantom for all image types. Nominal significance could not be assessed based on the quantitative variance results due to the distribution's right skewness.

mAs was identified as a major variance contributor to iodine quantification error for the 15 mg/mL insert in the DEQC body phantom, while mA was identified as a major variance contributor to iodine quantification error for the 5 mg/mL insert in the DEQC head phantom. Neither were found to be nominally significant.

Iodine quantification results for both the DEQC head and body phantoms are shown in Fig. 3. For the DEQC body phantom, increased mAs results in lower absolute error in iodine quantification and smaller variation within the collected data. For the DEQC head phantom, tube current has a minimal effect on iodine quantification error and does not seem to influence the variation in the collected data. The absolute error in the iodine quantification was generally less than 1.5 mg/mL for the DEQC body phantom and less than 0.3 mg/mL for the DEQC head phantom. Neither effect was found to be nominally significant (Table IX).

Monoenergetic HU stability results based on mAs for both the DEQC body and head phantoms are shown in Fig. 4. For the DEQC body phantom, mAs was shown to have a nominally significant impact on all monoenergetic reconstructions apart from 70 keV. The spectral separation between the reconstructions is markedly reduced at 208 mAs and below and increases slightly from 315 to 600 mAs. Standard deviation across the data points is also greatly reduced in the higher mAs range.

Noise results within the brain material insert based on CTDIvol for both the DEQC head and body phantoms are



TABLE IX. Results for DEQC Protocol 2. Technique parameters found to be major variance contributors for combinations of test metric and image type for both the DEQC head and body phantoms. Underlined text represents those technique parameters further assessed to have a nominally significant effect on the test result for a given image type. Blank cells indicate invalid combinations of test metric and image type, while hyphens indicate combinations where none of the investigated technique parameters were found to be major variance contributors.

Phantom	Test metric	50 keV	70 keV	110 keV	140 keV	I(Wa)	Wa(I)
DEQC body phantom	Iodine quant error 2 mg/mL					-	-
	Iodine quant error 5 mg/mL					-	-
	Iodine quant error 15 mg/mL					mAs	-
	Monoenergetic HU stability	<u>mAs</u>	-	<u>mAs</u>	<u>mAs</u>	-	-
	Noise <sup>a</sup>	CTDIvol	CTDIvol	CTDIvol	CTDIvol	CTDIvol	CTDIvol
	Positional constancy	<u>mAs</u>	-	<u>mAs</u>	<u>mAs</u>	mAs	<u>mAs</u>
DEQC head phantom	Iodine quant error 2 mg/mL					-	-
	Iodine quant error 5 mg/mL					mA	-
	Monoenergetic HU stability	-	-	<u>mAs</u>	<u>mAs</u>	-	-
	Noise <sup>a</sup>	CTDIvol, mA	CTDIvol, mA	CTDIvol, mA	CTDIvol, mA	CTDIvol, mA	CTDIvol, mA
	Positional constancy	-	-	mA	mA	mA	mA

<sup>a</sup>The nominal significance of CTDIvol and mAs on noise cannot be assessed using this method due to the log transformation of the data.

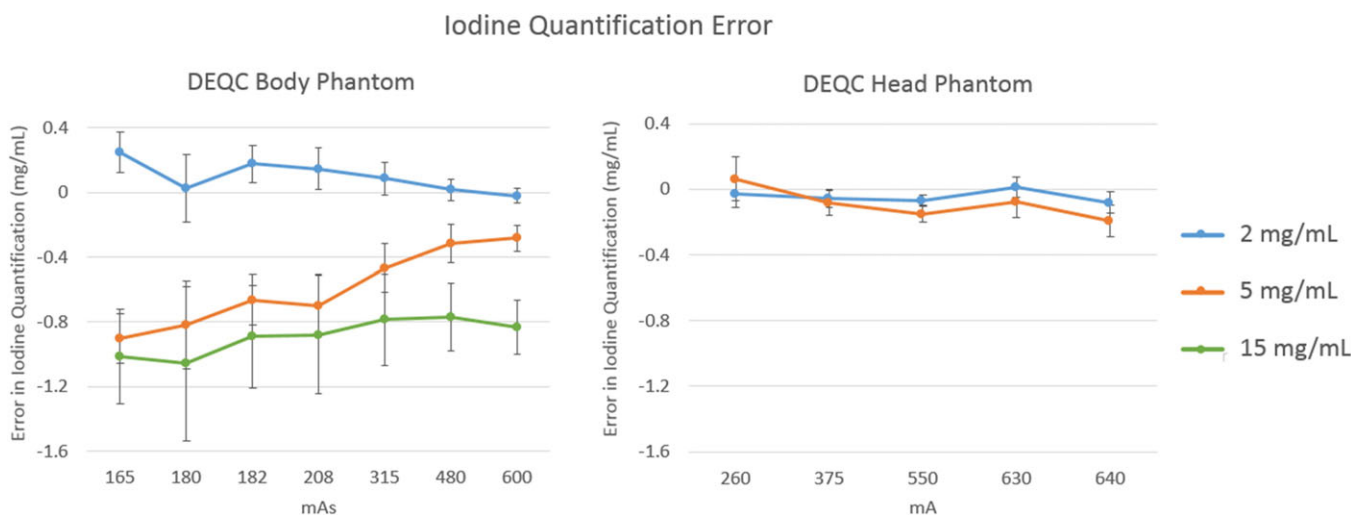


FIG. 3. Iodine quantification error measured on the Iodine (Water) images for the technique parameter isolated as a major variance contributor in Table IX: mAs for the DEQC body phantom (left) and mA for the DEQC head phantom (right). Iodine quantification error was measured as the difference between the nominal and measured iodine concentration for all iodine inserts present (see Fig. 1 for iodine insert positioning). Error bars represent standard deviation across 10 scanners and 13 weeks.

shown in Fig. 5. Results for monoenergetic and material density reconstructions are shown separately due to the different units and ranges of interest. Unsurprisingly, increased CTDIvol resulted in reduced noise for all reconstructions and in both phantoms. While 50 keV reconstructions resulted in much greater noise than the higher energy reconstructions, noise results varied less with reconstruction energy for the DEQC head phantom. Although mA was also identified as a major variance contributor to noise, plotting noise by this technique parameter alone did not elucidate any trends based on mA.

Positional constancy results by mAs for the DEQC body phantom and by mA for the DEQC head phantom are shown in Fig. 6. For the DEQC head phantom, increasing mA resulted in improved positional constancy for material density and monoenergetic reconstructions. The 70 keV reconstructions resulted in optimized constancy regardless of mA. For the DEQC body phantom, 70 keV constancy was consistent

across mAs values but the distribution of results was centered at 4–5 HU rather than the ideal of 0 HU. Positional constancy values for different monoenergetic reconstructions approached 70 keV results as mAs was increased, converged at 400 mAs and subsequently diverged at 600 mAs. A discontinuity in this trend is observed at 315 mAs corresponding to GSI-preset 1 (Table IX). Standard deviation across the data points is also reduced for 315 mAs and higher.

## 4. DISCUSSION

### 4.A. DEQC protocol version 1: Identification of relevant technique parameters

The results of protocol version 1 (Table VII) allowed for a more targeted investigation into technique parameters relevant to the scanners dual-energy performance. Both CTDIvol

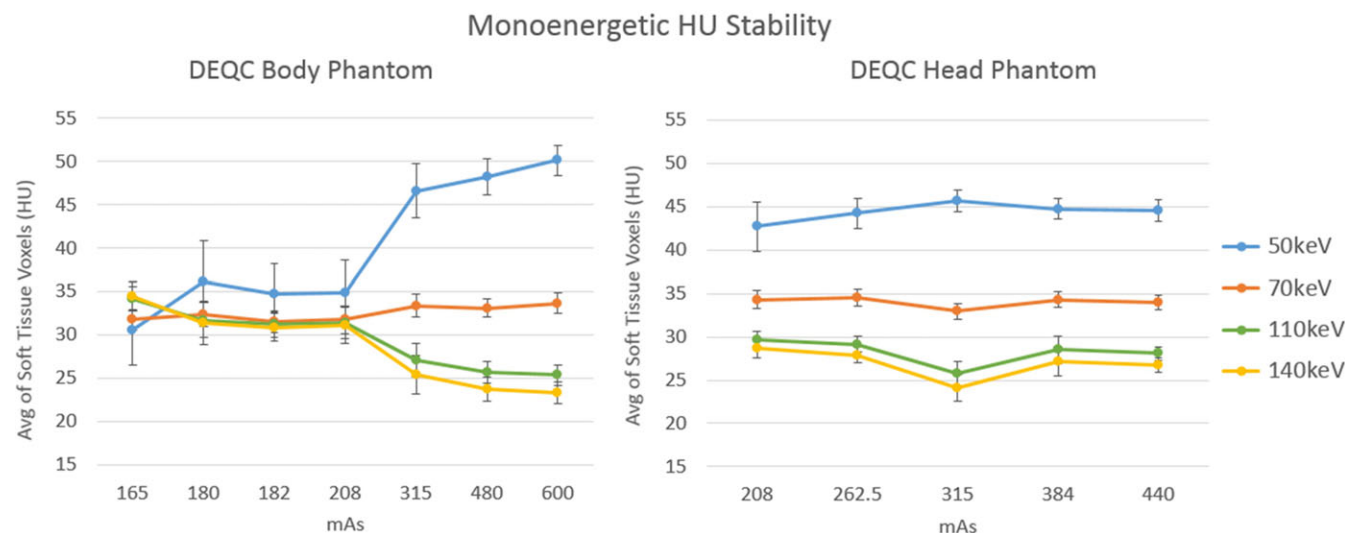


FIG. 4. Monoenergetic HU Stability plotted by the technique parameter isolated as a major variance contributor in Table IX: mAs for both the DEQC body (left) and head phantom (right). Results are shown for all monoenergetic reconstructions investigated (50, 70, 110 and 140 keV). Monoenergetic HU Stability is represented as the average of all voxels across the soft tissue inserts in the phantom (see Fig. 1 for soft tissue insert positioning). Error bars represent standard deviation across 10 scanners and 13 weeks.

and rotation time were found to have statistically and nominally significant effects on monoenergetic HU stability, noise, and positional constancy. Of particular interest, iodine quantification error was not affected by any of the technique parameters in a nominally significant manner. This result is encouraging for the quantitative use of dual-energy CT across a range of protocol variations.

While both pitch and image thickness had a statistically and nominally significant effect on noise, these technique parameters were not targeted for further investigation. The effect of image thickness on noise has been well characterized<sup>33</sup> and it is unlikely that the relationship between these technique parameters and noise would be affected by the material decomposition process. While pitch was found to have a statistically and nominally significant effect on noise, the effects of pitch are unfortunately convoluted with those of CTDIvol. Unlike single-energy acquisitions where the various technique parameters can be modified individually, dual-energy acquisitions using this scanner model are limited to a number of presets comprised of fixed bowtie filter, collimation, rotation time and CTDIvol. Given these constraints, variation in pitch was used as a driver for variation in CTDIvol, limiting the utility of independent investigation of pitch as an influential factor. For the DEQC body phantom protocol, the average CTDIvol for the 0.516 pitch was 41 mGy, while the average CTDIvol for 0.984 pitch was 22 mGy. For the DEQC head phantom protocol, the average CTDIvol for the 0.531 pitch was 94 mGy, while the average CTDIvol for 0.969 pitch was 51 mGy. Given the difficulty of evaluating effects of pitch separate from CTDIvol, and the fact that this effect was limited to noise (where the effect of CTDIvol is the most substantial) it was decided to focus further investigation on CTDIvol and rotation time.

## 4.B. DEQC protocol version 2: Scanner characterization

### 4.B.1. Iodine quantification error

Iodine quantification error was measured for several iodine concentration levels over a wide range of technique parameters. A statistically significant effect on iodine quantification error was found for one rod in each phantom: the 15 mg/mL rod in the DEQC body phantom, and the 5 mg/mL rod in the DEQC head phantom. These were the highest iodine concentration inserts present in each phantom configuration. This effect is likely due to the local environment of the rod; however, this cannot be assessed given the current data and is beyond the scope of the study. There was a slight trend toward improved accuracy at higher mAs; however, this effect was not found to be statistically significant. In fact, despite the wide range of values investigated, none of the technique parameters were identified as having a nominally significant effect on iodine quantification error. Iodine quantification error was generally less than 1.5 mg/mL in the DEQC body phantom and less than 0.3 mg/mL in the DEQC head phantom.

Several studies have been performed investigating the effects of position within the phantom,<sup>13</sup> rotation time,<sup>34</sup> phantom size,<sup>35</sup> and iodine concentration<sup>13,34,35</sup> on iodine quantification error. Studies using fast-switching DECT technology have shown that iodine quantification error was greater at the phantom base (6 o'clock position relative to center and other peripheral positions) and with 0.6 s rotation time (relative to 0.8 and 1 s). The potential impact of the positional dependency on iodine quantification error in this study cannot be directly assessed using the data collected as none of the inserts investigated were positioned at the

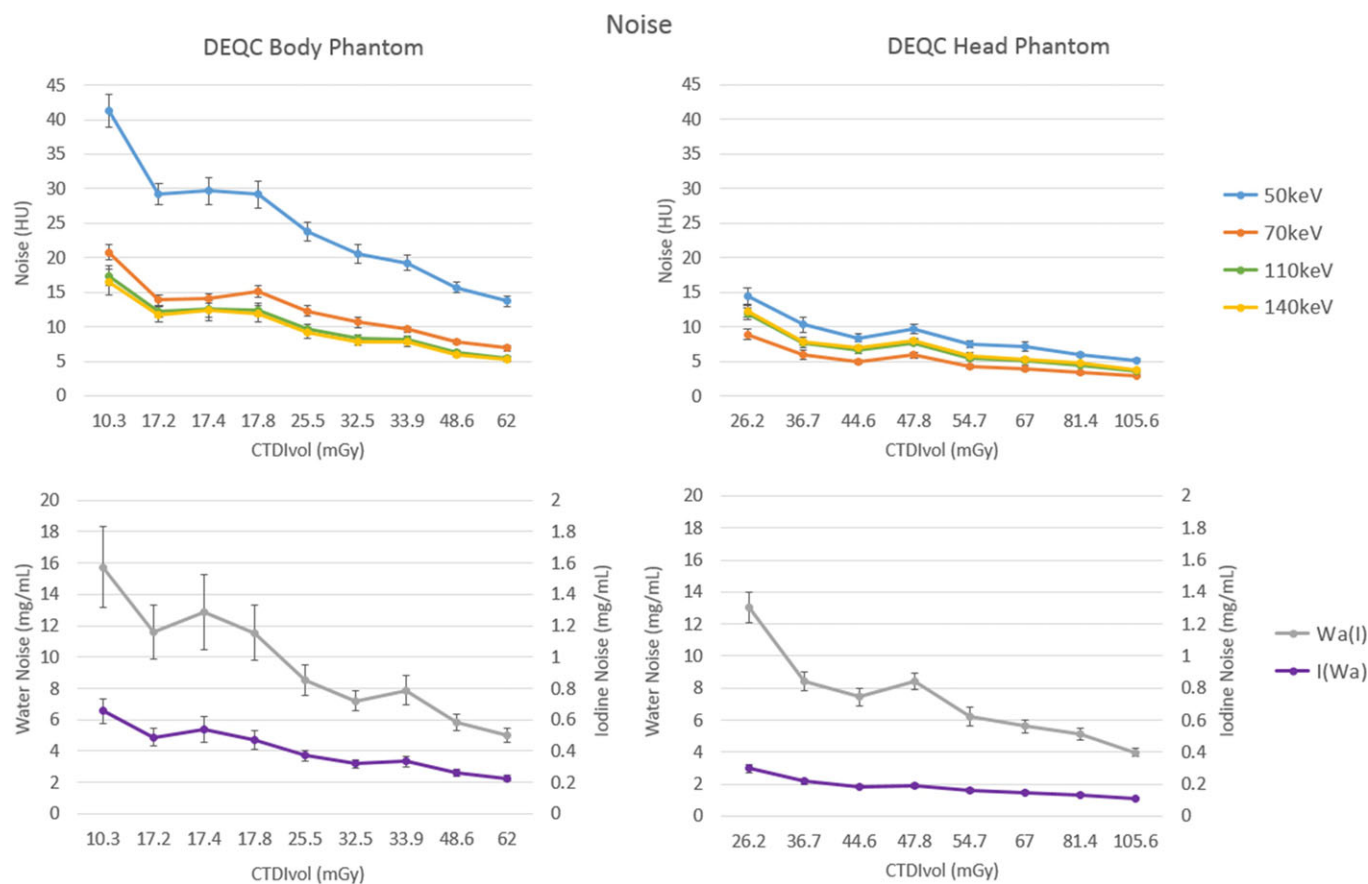


FIG. 5. Noise plotted by the technique parameter isolated as major variance contributors in Table IX: CTDIvol for the DEQC body phantom for both monoenergetic (upper left) and material density reconstructions (lower left). Noise was measured as the standard deviation within the brain material insert (see Fig. 1 for brain insert positioning). Error bars represent standard deviation across 10 scanners and 13 weeks.

phantom's base. While our results do not show a direct correlation between iodine quantification error and rotation time, the effect of mAs on this test metric was seen in the DEQC body phantom.

Although dual-source, split-filter, and dual-layer detector DECT technologies feature very different data acquisition methods from the fast switching method used in this paper, studies across DECT platforms report iodine quantification error increasing with iodine concentration and phantom size.<sup>23,36,37</sup> In our study, we found that across all 10 DECT scanners, iodine quantification errors were reported to be within 5%–10%, corresponding to  $\pm 0.3$  and  $\pm 1.5$  mg/mL for the 2 and 15 mg/mL inserts, respectively. This low error and the low dependence on the technique parameters investigated, suggest that iodine density maps may be used in a quantitative manner for clinically relevant iodine concentrations regardless of the technique parameters used.<sup>30</sup>

#### 4.B.2. Monoenergetic HU stability

Monoenergetic stability was found to be both statistically and clinically affected by variation in mAs. Graphing this relationship helped highlight the dramatic effect of protocol

mAs on the utility of monoenergetic imaging. Protocols employing less than 315 mAs resulted in very similar CT numbers across all monoenergetic reconstructions investigated. One of the greatest advantages of dual-energy CT over single-energy CT is the variable contrast based on reconstructed keV that is derived from the dual-energy data. However, in order to acquire dual-energy data, both the 80 and 140 kVp beams must penetrate through the patient in sufficient quantities to be reconstructed into an image. In the case of the DEQC body phantom, it is likely that protocols below 315 mAs did not provide sufficient tube output to result in adequate photon collection at the detector for the 80 kVp beam. Having limited 80 kVp data to draw from, the material decomposition process was highly affected, resulting in fixed CT numbers across all monoenergetic reconstructions (Fig. 4). To our knowledge, this is the first study to demonstrate the reduced utility of monoenergetic images, and dual-energy acquisition in general, in larger patient sizes when aggressive tube current reduction is employed. While it is clear that the loss of the 80 kVp beam occurred between 208 and 315 mAs for this particular object's size and shape, the specific mAs necessary for adequate penetration cannot be determined from the data collected. In addition, the mAs required for material decomposition likely is not static but

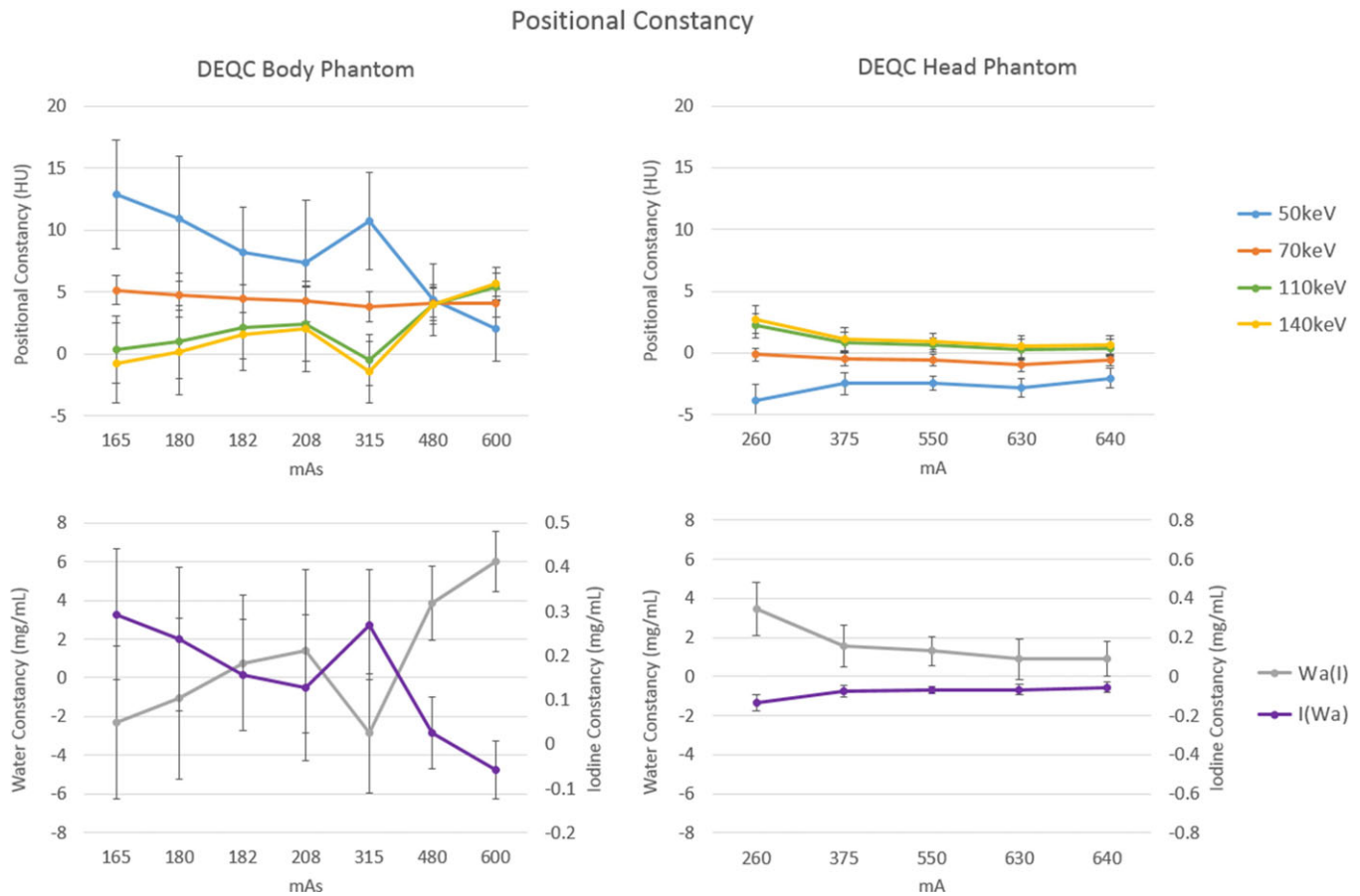


FIG. 6. Positional constancy plotted by the technique parameter isolated as a major variance contributor in Table IX: mAs for the DEQC body phantom for monoenergetic (upper left) and material density reconstructions (lower left); and mA for the DEQC head phantom for monoenergetic (upper right) and material density reconstructions (lower right). Positional constancy was measured as the difference between the peripheral and central soft tissue rod (see Fig. 1 for soft tissue insert positioning). Error bars represent standard deviation across 10 scanners and 13 weeks.

highly dependent on patient size. Therefore, attempts at dose reduction in DECT protocols should be pursued with particular attention to ensuring adequate tube current to avoid material decomposition collapse and the resulting uniform contrast across monoenergetic reconstructions.

Monoenergetic stability was also found to be both statistically and nominally effected by mAs in the DEQC head phantom. Unlike the DEQC body phantom, all mAs values provided spectral separation from successful material decomposition. In fact, the attenuation measures from the monoenergetic reconstructions appear remarkably stable with the exception of the 315 mAs station (Fig. 4). This mAs value corresponds with a combination of the lowest rotation time (0.5 s) and one of the highest mA levels (630 mA) available for use in dual-energy mode. While independent verification proved elusive, it is hypothesized that this lowest rotation time has a detrimental effect on spectral separation between the 80 and 140 kVp datasets. The time spent switching between kVp levels is independent of rotation time, and data are collected continuously. For a low rotation time, the switching time represents a larger fraction of the waveform period than at higher rotation times, potentially rounding the waveform and degrading spectral separation.

#### 4.B.3. Noise

While variance component analysis isolated both CTDIvol and mA as major variance contributors in the DEQC head phantom, graphs of these relationships highlighted the strong effect of CTDIvol on image noise (Fig. 5). For both the DEQC head and body phantoms, increasing CTDIvol led to decreased image noise. This is a direct result of Poisson statistics as the increase in CTDIvol led to an increase in photons at the detector. Both monoenergetic and iodine/water material density image types followed this relationship. Although both iodine and water material density maps can be expressed in mg/mL, the fundamental nature of said units (mg/mL of iodine, representing the high-Z component of the attenuation, for iodine density images and mg/mL of water, representing the low-Z component of the attenuation, for water density images) invalidates direct comparison of the values. It is worth noting the greater disparity between 50 and 70 keV, 110 and 140 keV images for the DEQC body phantom, relative to the more uniform results for the DEQC head phantom. This could again be a consequence diminished penetration of the 80 kVp beam for the much larger DEQC body phantom; however, without direct access to the 80 kVp image that cannot be confirmed at this time.



#### 4.C. Positional constancy

For the DEQC head phantom, positional constancy (peripheral soft tissue CT number — central soft tissue CT number) improves and converges across monoenergetic reconstructions as the mA is increased (Fig. 6); however, this effect was not found to be nominally significant. While this same convergence is seen in the DEQC body phantom as mAs is increased, the positional constancy does not converge to zero, but to approximately 5 HU. At all mAs stations, the 70 keV reconstruction's constancy metric is static at approximately 5 HU. Given the low variability in the result across the dataset, representative of extensive data collection using 10 different scanners, it is reasonable to assume that this is not the result of a calibration error or need for service. It is likely, therefore, that this offset is a consequence of an intended setting or calibration resulting in suboptimal beam hardening correction. Of particular note is the discontinuity at 315 mAs. As noted above, this mAs station corresponds to a combination of the lowest rotation time (0.5 s) and highest mA (630) available in dual-energy imaging mode.

#### 4.D. Global discussions

Over the course of our investigation it became apparent that 70 keV reconstructions provided better results for most test metrics compared to the other monoenergetic levels investigated. In the case of noise, 70 keV images provided equivalent, or in the case of the DEQC head phantom, superior results compared to 50, 110, or 140 keV reconstructions. For both monoenergetic HU stability and uniformity, 70 keV reconstructions were less effected by variations in technique parameters, and in the case of the uniformity, provided more optimized results. In addition, for both initial (protocol version 1) and detailed (protocol version 2) investigations, statistical and nominal effects seen at 50, 110, and 140 keV were often not valid for 70 keV reconstructions. These results suggest that 70 keV reconstructions provide more consistent image quality across a wider range of technique parameters than any of the other monoenergetic reconstructions investigated. Several prior studies have noted that 68–70 keV reconstructions provide optimized noise and contrast-to-noise ratio.<sup>6,10,17</sup>

#### 4.E. Differences in DEQC body and head phantom results

In general, the DEQC head phantom provided more stable and improved results over the DEQC body phantom (Fig. 3). This is likely due to the difference in the penetration ability of the 80 kVp beam in the larger, elliptical DEQC body phantom versus the smaller, circular DEQC head phantom over the range of mAs stations available on the scanner. Iodine accuracy results for the DEQC head phantom showed 60% improvement in iodine accuracy relative to the DEQC body phantom. Monoenergetic HU stability results were dramatically improved in the DEQC head phantom due to the

lack of over-attenuation of the 80 kVp beam (Fig. 4). After eliminating those protocols with inadequate transmission, the results for attenuation (HU) range across protocols were similar for both phantoms. While the DEQC body phantom provided inconsistent results on the effect of protocol mAs on positional constancy (Fig. 6), the DEQC head phantom provided steady improvement in measured constancy with increasing protocol mAs. In addition, the positional constancy for 50 keV monoenergetic reconstructions was vastly improved from a maximum value of 18 HU in the DEQC body phantom to 5 HU in the DEQC head phantom.

#### 4.F. Limitations

The exploratory and comprehensive nature of this investigation resulted in a very heterogeneous phantom that limited the application of some test metrics. While a more uniform phantom would have allowed direct use of the more traditional definitions of some of the test metrics, for example noise and uniformity, modifications of these metrics allowed for investigation of a wide range of endpoints and acquisition techniques in the more heterogeneous phantom. These test metric modifications have been discussed extensively in the methods section and should be considered when interpreting the results.

While efforts were made to mimic relevant patient sizes and both head and body anatomy, certain features of the DEQC head and DEQC body phantoms should be noted. First, in order to include relevant material rods, the size of the DEQC head phantom was increased to 22 cm, larger than the diameter of the typical human head, which measures approximately 17 cm on average.<sup>38</sup> Second, the profile of the DEQC head phantom was simplified to a circle, enabling easy insertion and removal from the DEQC body phantom. Third, the DEQC head phantom was not designed with anthropomorphic features like a skull, which would influence its applicability to patient scans. Due to its size and shape, the DEQC head phantom was imaged on a stand on the CT tabletop instead of in a head holder, which would better approximate clinical imaging. For both the DEQC head and body phantoms, material rods were fixed to a single location. Although an attempt was made to optimize the rod layout to minimize the effect of beam hardening on the evaluation of test metrics, it is likely that test metric results were influenced by both a rod's location and local environment. This is especially true for noise, which was evaluated within a single centrally located rod and not over a larger or more representative portion of the phantom. Iodine quantification error was assessed using a material decomposition of pure iodine and water, although the rods were fabricated by adding iodobenzene (C<sub>6</sub>H<sub>5</sub>I) to a 0 HU epoxy resin material. This discrepancy between the fabrication materials and the basis materials for the material decomposition may influence the accuracy of the iodine concentration results. Finally, ground truth for iodine quantification error was derived from the stated iodine concentration by the rod manufacturer. Without a method of independent verification, errors in iodine quantification error

could potentially be confounded by errors in rod fabrication. In addition to the phantoms, analysis was limited by the inability to independently investigate technique parameters due to the use of fixed GSI-presets.

Given the differences in acquisition and analysis methods between the various DECT manufacturers, it is important to note that the results of this study are specific to fast-kVp switching and should not be generalized to dual-source, split-filter, or dual layer scanners. Additionally, enhancements to fast-kVp switching acquisition or modification to the material decomposition or post processing may affect these results. As such, the conclusions of this study are specific to the GE 750HD DECT system. And finally, thresholds utilized for statistical analysis in this study were established based on single-energy QC equivalences and manufacturer tolerances and are therefore individually defined for all image types.

## 5. CONCLUSIONS

Although a scan protocol covering the full range of multiple parameters is essential for the full characterization of a system, long-term collection of such data is impractical. To develop a protocol for the long-term collection of quality control data, a streamlined protocol was developed based on the results from the 13 weeks of DEQC analysis (Table X). Given the stronger impact of acquisition parameters on test metrics using the DEQC body phantom, relative to results in the DEQC head phantom, and the current increase of DECT applications in the body relative to the head, long-term data collection was limited to the DEQC body phantom. Facilities specializing in neurological applications of DECT technology may benefit more from extended data collection using the DEQC head phantom. Phantom scanning was limited to six acquisitions covering a more clinical CTDI<sub>vol</sub> range of 17.2–33.9 mGy, while maintaining those acquisitions necessary to separate effects due to CTDI<sub>vol</sub> and rotation time. The authors recommend that DECT QC be performed on a monthly basis; however, weekly assessment is encouraged if logistically feasible for the facility. This more limited

TABLE X. Recommendations for long-term data collection to determine baseline values and tolerances necessary for the establishment of a DECT quality control program. All acquisitions apply to the DEQC body phantom and are performed in helical scan mode, using a 40 mm beam width, Large Body SFOV, 42 cm DFOV, and standard reconstruction filter.

Acquisition	GSI-preset	Pitch	Rotation time (s)	mA	Image thickness (mm)	CTDI <sub>vol</sub> (mGy)
1	GSI-1	0.516	0.5	630	5	33.9
2	GSI-5	0.984	1	600	5	32.5
3	GSI-10	0.984	0.8	600	5	25.5
4	GSI-1	0.984	0.5	630	5	17.8
5	GSI-54	0.516	0.6	275	5	17.4
6	GSI-48	0.516	0.7	260	5	17.2

protocol will allow for the more routine and long-term data collection crucial to the determination of baseline values and statistically based failure thresholds necessary for the establishment of a DECT quality control program.

## 5.A. Future work

Future work includes development of a dual-energy quality control process for split-filter dual-energy systems, dual-source dual-energy systems, and dual-layer detector dual-energy systems. In addition, investigation will continue into the effect of phantom (or patient) size on the mAs threshold to avoid uniform contrast across monoenergetic reconstructions (Fig. 4), as well as the creation of a more advanced and rigorous noise metric. Data will continue to be collected in order to determine baseline values and failure threshold criteria for the validation of long-term DECT scanner performance.

## ACKNOWLEDGMENTS

The authors thank Jim Pennington for his contribution to the design and fabrication of the DEQC phantom system, Cristel Baiu of Gammex for the development of the material and tissue inserts, and Adam Chandler of GE for his technical expertise and support of this project. The authors also thank John Rong and Xinming Liu for their logistic and intellectual support. Statistical analysis was funded in part by the NIH (NIH CCSG grant # P30 CA016672). Partial salary support was provided by Dr. William Murphy, Jr., MD, the John S. Dunn, Sr. Distinguished Chair in Diagnostic Imaging at MD Anderson Cancer Center, Houston, TX, USA.

## CONFLICT OF INTEREST

This research was conducted with the MD Anderson Center for Advanced Biomedical Imaging in part with equipment support from General Electric Healthcare.

\*Present address: Department of Environmental Health and Safety, Cedars Sinai Medical Center, Los Angeles, CA, 90048, USA

<sup>a)</sup>Author to whom correspondence should be addressed. Electronic mail: dcody@mdanderson.org

## REFERENCES

- Cody D, Pfeiffer D, McNitt-Gray M, Ruckdeschel T, Strauss K. *Computed Tomography: Quality Control Manual*. (Radiology AC of, ed.). Virginia: American College of Radiology; 2012.
- Langan DA, *Gemstone Spectral Imaging: GE White Paper*. Waukesha, WI: GE Health care; 2008.
- Flohr TG, McCollough CH, Bruder H, et al. First performance evaluation of a dual source CT (DSCT) system first performance evaluation of a dual source CT system. *Eur Radiol*. 2006;16:256–268.
- Primak AN, Ramirez Giraldo JC, Liu X, Yu L, McCollough CH. Improved dual-energy material discrimination for dual-source CT by means of additional spectral filtration. *Med Phys*. 2009;36:1359–1369.
- Kaza RK, Platt JF, Megibow AJ. Dual-energy CT of the urinary tract. *Abdom Imaging*. 2013;38:167–179.

6. Yu L, Leng S, McCollough CH. Dual-energy CT-based monochromatic imaging. *AJR Am J Roentgenol.* 2012;199(5 Suppl):S9–S15.
7. Kalender WA, Perman WH, Vetter JR, Klotz E. Evaluation of a prototype dual-energy computed tomographic apparatus. I. Phantom Studies. *Med Phys.* 1986;13:334–339.
8. Fletcher JG, Takahashi N, Hartman R, et al. Dual-energy and dual-source CT: is there a role in the abdomen and pelvis? *Radiol Clin North Am.* 2009;47:41–57.
9. Alvarez RE, Macovski A. Energy-selective reconstructions in X-ray computerized tomography. *Phys Med Biol.* 1976;21:733–744.
10. Matsumoto K, Jinzaki M, Tanami Y, Ueno A, Yamada M, Kuribayashi S. Virtual monochromatic spectral imaging with fast kilovoltage switching: improved image quality as compared with that obtained with conventional 120-kVp CT. *Radiology.* 2011;259:257–262.
11. Yuan R, Shuman WP, Earls JP, et al. Reduced iodine load at ct pulmonary angiography with dual-energy monochromatic imaging: comparison with standard CT pulmonary angiography—a prospective randomized trial. *Radiology.* 2012;262:290–297.
12. Yu L, Christner JA, Leng S, Wang J, Fletcher JG, McCollough CH. Virtual monochromatic imaging in dual-source dual-energy CT: radiation dose and image quality. *Med Phys.* 2011;38:6371–6379.
13. Zhang D, Li X, Liu B. Objective characterization of GE Discovery CT750 HD scanner: gemstone spectral imaging mode. *Med Phys.* 2011;38:1178–1188.
14. Lin XZ, Miao F, Li JY, Dong HP, Shen Y, Chen KM. High-definition CT Gemstone spectral imaging of the brain: initial results of selecting optimal monochromatic image for beam-hardening artifacts and image noise reduction. *J Comput Assist Tomogr.* 2011;35:294–297.
15. Yamada Y, Jinzaki M, Tanami Y, Abe T, Kuribayashi S. Virtual Monochromatic Spectral Imaging for the Evaluation of Hypovascular Hepatic Metastases. *Invest Radiol.* 2012;47:292–298.
16. Li B, Yadava G, Hsieh J. Quantification of head and body CTDI(VOL) of dual-energy x-ray CT with fast-kVp switching. *Med Phys.* 2011;38:2595–2601.
17. Pomerantz SR, Kamalian S, Zhang D, et al. Virtual monochromatic reconstruction of dual-energy unenhanced head CT at 65-75 keV maximizes image quality compared with conventional polychromatic CT. *Radiology.* 2013;266:318–325.
18. Lee YH, Park KK, Song H-T, Kim S, Suh J-S. Metal artefact reduction in gemstone spectral imaging dual-energy CT with and without metal artefact reduction software. *Eur Radiol.* 2012;22:1331–1340.
19. Bamberg F, Dierks A, Nikolaou K, Reiser MF, Becker CR, Johnson TR. Metal artifact reduction by dual energy computed tomography using monoenergetic extrapolation. *Eur Radiol.* 2011;21:1424–1429.
20. Zhou C, Zhao YE, Luo S, et al. Monoenergetic imaging of dual-energy CT reduces artifacts from implanted metal orthopedic devices in patients with fractures. *Acad Radiol.* 2011;18:1252–1257.
21. Lewis M, Reid K, Toms AP. Reducing the effects of metal artefact using high keV monoenergetic reconstruction of dual energy CT (DECT) in hip replacements. *Skeletal Radiol.* 2013;42:275–282.
22. Meinel FG, Bischoff B, Zhang Q, Bamberg F, Reiser MF, Johnson TR. Metal artifact reduction by dual-energy computed tomography using energetic extrapolation: a systematically optimized protocol. *Invest Radiol.* 2012;47:406–414.
23. Chandarana H, Megibow AJ, Cohen BA, et al. Iodine quantification with dual-energy CT: phantom study and preliminary experience with renal masses. *Am J Roentgenol.* 2011;196:W693–W700.
24. Feuerlein S, Heye TJ, Bashir MR, Boll DT. Iodine quantification using dual-energy multidetector computed tomography imaging: phantom study assessing the impact of iterative reconstruction schemes and patient habitus on accuracy. *Invest Radiol.* 2012;47:656–661.
25. Koonce JD, Vliegenthart R, Schoepf UJ, et al. Accuracy of dual-energy computed tomography for the measurement of iodine concentration using cardiac CT protocols: validation in a phantom model. *Eur Radiol.* 2014;24:512–518.
26. Pelgrim GJ, van Hamersvelt RW, Willeminck MJ, et al. Accuracy of iodine quantification using dual energy CT in latest generation dual source and dual layer CT. *Eur Radiol.* 2017;27:3904–3912.
27. Kawai T, Takeuchi M, Hara M, et al. Accuracy of iodine removal using dual-energy CT with or without a tin filter: an experimental phantom study. *Acta Radiol.* 2013;54:954–960.
28. Karlo C, Lauber A, Gotti RP, et al. Dual-energy CT with tin filter technology for the discrimination of renal lesion proxies containing blood, protein, and contrast-agent. An experimental phantom study. *Eur Radiol.* 2011;21:385–392.
29. Matsuda I, Akahane M, Sato J, et al. Precision of the measurement of CT numbers: comparison of dual-energy CT spectral imaging with fast kVp switching and conventional CT with phantoms. *Jpn J Radiol.* 2012;30:34–39.
30. Jacobsen MC, Schellingerhout D, Wood CA, et al. Intermanufacturer comparison of dual-energy CT iodine quantification and monochromatic attenuation: a phantom study. *Radiology.* 2017:170896.
31. Kayugawa A, Ohkubo M, Wada S. Accurate determination of CT point-spread-function with high precision. *J Appl Clin Med Phys.* 2013;14:3905.
32. General Electric Healthcare. Discovery CT750 HD Technical Reference Manual. 2012:176–177. [http://www3.gehealthcare.com/en/support/support\\_documentation\\_library](http://www3.gehealthcare.com/en/support/support_documentation_library).
33. Brooks RA, di Chiro G. Statistical limitations in x-ray reconstructive tomography. *Med Phys.* 1976;3:237–240.
34. Wang L. Can gemstone spectral imaging accurately determine the concentration of iodine contrast: a phantom study. *Omi J Radiol.* 2013;2:1000141.
35. Marin D, Pratts-Emanuelli JJ, Mileto A, et al. Interdependencies of acquisition, detection, and reconstruction techniques on the accuracy of iodine quantification in varying patient sizes employing dual-energy CT. *Eur Radiol.* 2015;25:679–686.
36. Li JH, Du YM, Huang HM. Accuracy of dual-energy computed tomography for the quantification of iodine in a soft tissue-mimicking phantom. *J Appl Clin Med Phys.* 2015;16:418–426.
37. Euler A, Parakh A, Falkowski AL, et al. Initial results of a single-source dual-energy computed tomography technique using a split-filter: assessment of image quality, radiation dose, and accuracy of dual-energy applications in an in vitro and in vivo study. *Invest Radiol.* 2016;51:491–498.
38. Bushby KM, Cole T, Matthews JN, Goodship JA. Centiles for adult head circumference. *Arch Dis Child.* 1992;67:1286–1287.